ARTICLE

Lock-in Amplifier Based Peak Force Infrared Microscopy

Andrea Dorsa,[a] Qing Xie,[a] Martin Wagner,[b] and Xiaoji G. Xu [a*]

Received 00th January 20xx,
Accepted 00th January 20xx

DOI: 10.1039/x0xx00000x

Nanoscale infrared (nano-IR) microscopy enables label-free chemical imaging with a spatial resolution below Abbe's diffraction limit through the integration of atomic force microscopy and infrared radiation. Peak force infrared (PFIR) microscopy is one of the emerging nano-IR methods that provides non-destructive multimodal chemical and mechanical characterization capabilities using a straightforward photothermal signal generation mechanism. PFIR microscopy has been demonstrated to work for a wide range of heterogeneous samples, and it even allows operation in the fluid phase. However, the current PFIR microscope requires customized hardware configuration and software programming for real-time signal acquisition and processing, which creates a high barrier to PFIR implementation. In this communication, we describe a type of lock-in amplifier-based PFIR microscopy that can be assembled with generic, commercially available equipment without special hardware or software programming. We demonstrate this method on soft matters of structured polymer blends and blocks, as well as biological cells of *E. coli*. The lock-in amplifier-based PFIR reduces the entry barrier for PFIR microscopy and makes it a competitive nano-IR method for new users.

Introduction

Infrared (IR) spectroscopy and microscopy are convenient and non-invasive analytical techniques for identifying chemical compositions. However, Abbe's diffraction limit prevents traditional infrared microscopy from reaching nanoscale spatial resolution[1]; therefore, nanoscale heterogeneous samples, such as structured polymers and biological cells, cannot be easily resolved spatially with infrared microscopy. Atomic force microscopy (AFM) was combined with infrared radiation to bypass the optical diffraction limit, leading to the development of two popular families of AFM-based IR methods. The first family, scattering-type scanning near-field optical microscopy (s-SNOM), is based on the optical detection of scattered light from the near field of a sharp metallic AFM tip near the sample.[2, 3] s-SNOM delivers 10~20 nm spatial resolution. It is a widely used technique to study heterogeneous samples with strong spatial contrast of dielectric functions and two-dimensional materials that support polaritons.[4]

The other family of methods, and an increasingly popular AFM-based infrared spectroscopy method for soft matters, is the AFM-IR, which mechanically detects the photothermal response of the sample due to IR absorption. Since its early conception and demonstration,[5, 6] AFM-IR has been developed with different AFM operational modes:[7] the original photothermal induced resonance (PTIR) technique that is based on contact mode,[8, 9] photo-induced force microscopy (PiFM),[10, 11] or tapping AFM-IR, that is based on tapping mode,[9, 12] and peak force infrared (PFIR) microscopy that is based on the peak tapping mode.[13, 14] These AFM-IR techniques inherit the same advantages and limitations of their respective AFM operational modes.

PFIR microscopy, a peak force tapping-based AFM-IR method, delivers a multimodal chemical and mechanical characterization platform. PFIR microscopy has been applied to a range of nanoscale heterogeneous samples, from polymers and biological specimens to oil shale source rock and polaritonic materials.[15-19] PFIR microscopy also enables nanoscale IR microscopy and spectroscopy in the liquid/aqueous phase,[20, 21] leveraging the suitability of peak force tapping mode in the fluid phase. Recent development of PFIR microscopy has been the integration of the surface potential mapping ability of pulsed force Kelvin probe force microscopy, which delivers simultaneous chemical, mechanical, and surface potential mapping in one AFM mode.[18] However, despite the successful demonstration of PFIR microscopy, its popularity is limited by the complexity of its customized signal generation and processing routine. A typical PFIR microscope requires hardware or software-level programming on signal acquisitions and processing, which often involves programming with LabVIEW or equivalent platforms. The necessity of mastering these programming tools for utilization creates an entry barrier for spectroscopists or analytical chemists. In contrast, both PTIR and PiFM/tapping AFM-IR can be assembled with standard commercially available hardware without programming. The

[a,a] *Department of Chemistry, Lehigh University, 6 E Packer Ave., Bethlehem, PA, 18015, United States*
[b,b] *Bruker Nano Surface, 112 Robin Hill Road, Santa Barbara, CA, 93117 United States*
† Corresponding email: xgx214@lehigh.edu
Electronic Supplementary Information (ESI) available: [details of any supplementary information available should be included here]. See DOI: 10.1039/x0xx00000x

data can be acquired with lock-in amplifiers in PTIR and PiFM/tapping AFM-IR.

How can the signal processing of PFIR microscopy be simplified to reduce the technical barrier to its wider adaptation? In this article, we describe our development of a lock-in amplifier-based variant of PFIR microscopy that can be assembled with commercially available instruments and without the necessity for customized hardware or software for signal acquisition and data processing.

Method

PFIR microscopy operates in peak force tapping (PFT) mode,[22] also known as pulsed force mode.[23] In PFT mode, the AFM tip intermittently indents into the sample surface under an external peak force set point regulated by a negative feedback loop. The PFT frequency is typically set at a low value, e.g., 4 kHz, which is much lower than that of the cantilever resonant frequency that the regular tapping mode operates at. PFIR inherits the advantages of PFT mode and is suitable to various samples of different moduli and surface roughness. Compared with traditional contact mode and tapping mode, PFT mode offers deterministic tip-sample contact, and at the same time, it avoids scratching the sample with the tip. As an AFM-IR method, PFIR utilizes the temporal regime when the tip and sample are in dynamic contact to measure the photothermal effect. The IR laser emissions are synchronized with the PFT cycle and adjusted to the moment when the tip and sample are in contact. The photothermal expansion of the sample causes the cantilever to deflect and oscillate, which in regular PFIR microscopy, is usually recorded by a data acquisition card with gated detection. The cantilever response due to the sample's photothermal expansion is then processed with customized software written in LabVIEW to obtain the PFIR signal in real-time. This real-time data treatment usually involves a Fast-Fourier Transform of the time-domain deflection trace with subsequent integration around the IR-induced cantilever oscillation frequencies.[13] The PFIR signal is recorded while the AFM tip scans over the sample to form a PFIR image. With regular PFIR operation, the challenge for widespread adaption is the customized signal acquisition and processing software, which is specific to certain hardware (e.g., a data acquisition card) and requires expertise in programming to achieve mastery.

To overcome this problem, our lock-in based PFIR microscopy instead uses a commercially available lock-in amplifier for data acquisition and processing, rather than requiring software or hardware-level programming. The apparatus consists of a peak force tapping enabled AFM (Multimode 8, Bruker Nano), an externally-triggerable mid-infrared quantum cascade laser in pulsed mode (QCL, MIRcat-QT, DRS Solutions), a multi-function lock-in amplifier (MPLi-5M-MF, Zurich Instruments), a function generator (HDG6112B, Hantek) and an assembly of standard optics. Figure 1a schematically illustrates the construction of the lock-in based PFIR microscope. The IR radiation beam from the QCL is expanded and guided to a parabolic mirror (Edmund Optics, effective focal length of 25.4 mm) mounted on a three-dimensional translation stage to position its focus on the AFM tip apex. The polarization of the IR light is parallel to the long axis of the AFM tip. The AFM operates at 4 kHz in peak force tapping frequency with a low peak force amplitude of 30 nm. A platinum-coated AFM tip (MikroMasch NSC:14/Pt) is used to enhance the IR radiation under its apex. The tip-enhanced infrared field excites the vibrational resonance of the sample and induces photothermal expansion. Since the pulsed duration of the QCL is at tens to hundreds of nanoseconds, the rapid photothermal expansion of the sample is capable of impulsively exciting the AFM cantilever, causing deflection and oscillation.

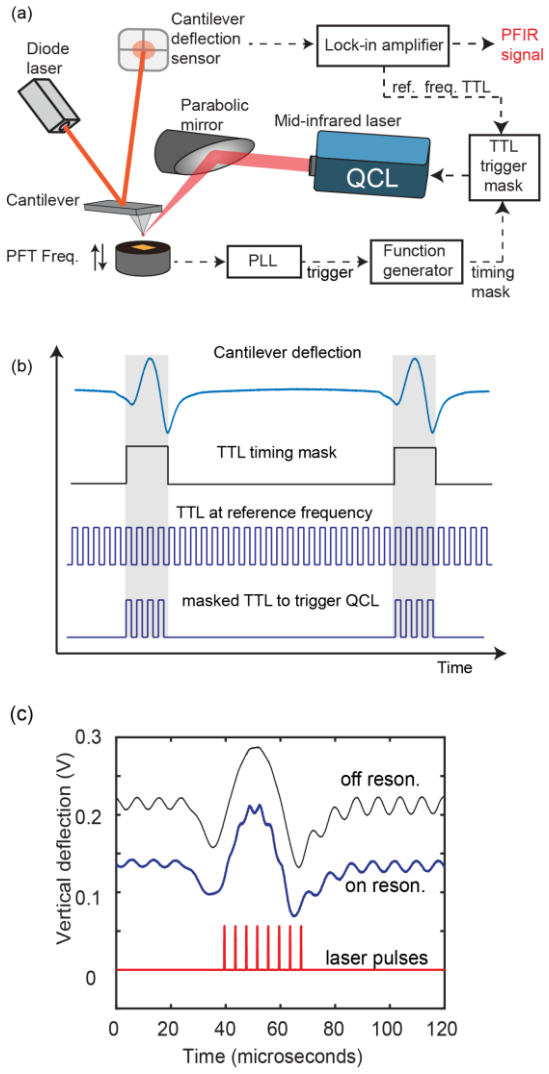

Figure 1. (a) The schematic illustration of the components of a lock-in-based PFIR microscope. (b) Schematic of excitation timing of the QC (c) Excitation scheme of the lock-in based PFIR microscopy. The black thin curve represents the cantilever's vertical deflection signals when the IR laser is tuned to be off resonance (1550 cm^{-1}) with the sample's IR absorption (polystyrene). The blue thick curve represents the cantilever's vertical deflection signal when the IR laser is on resonance (1493 cm^{-1}) with the polystyrene sample. Red lines represent the timing of laser pulses.

The magnitude of AFM cantilever deflection is detected by a quadrant diode from a laser beam reflected off the back of the cantilever.

In our development, the voltage waveform of the vertical deflection from the quadrant diode is routed to the one channel of the lock-in amplifier to generate a phase-locked transistor-to-transistor logic (TTL) waveform at the peak force tapping frequency *f*. The multichannel lock-in amplifier is acting as a phase locked loop (PLL). The TTL waveform triggers the function generator to produce a TTL pulse train, with the ON state synchronized with the peak force tapping cycle when the tip-sample is in contact. We call this TTL pulse train the TTL timing mask. We use the second channel of the lock-in amplifier to generation a high frequency TTL train at a reference frequency of F, which is the integer multiple of the peak force tapping frequency *f*. The value of F can be set at a range of high frequencies, so long as it avoids the cantilever free space oscillation frequency. In our case, the reference frequency is set to be around 1.4 times of the cantilever free space oscillation frequency. The TTL pulse train at F and the TTL time mask are then processed by a TTL trigger mask circuit that functions as a logic AND gate. The result of the operation is to only leave the TTL pulse ON when the tip sample are in momentary contact. The resulting TTL pulse train is routed to the QCL to trigger laser emissions. Timing of this operation is illustrated in Figure 1b. In this triggering configuration, there is no IR emission from the QCL when the tip and sample are not in contact during the PFT cycle, since the purpose is to avoid unnecessary background photothermal signals from heating the AFM cantilever alone, without the participation of the sample. The photothermal expansion of the sample due to IR absorption by the pulse train cause additional cantilever oscillations, as shown by Figure 1c. The vertical deflection signal waveform of the quadrant photodiode of the AFM is routed to the multichannel lock-in amplifier. The reference frequency for the lock-in detection is set at F, which is the repetition rate of the IR pulse train within each pack of emission.

Like other variations of PFIR microscopy, lock-in based PFIR microscopy has two operational modes: IR imaging and point spectroscopy. In the IR imaging mode, the QCL is set to a radiation frequency of interest, usually matching one of the functional groups of the sample. Then, the lock-in demodulation signal is recorded and routed to the AFM controller to be registered together with the AFM topography to create an image. In point spectroscopy, the AFM tip remains at one location of interest on the sample, and the radiation frequency of the QCL is swept while the lock-in demodulation signal is recorded. Correlating the lock-in signal with the IR frequency forms a nano-IR spectrum. Such spectrum collection can be done with a simple Labview software to swept IR frequency and record lock-in signal. Alternatively, one can use build-in data acquisition functionality of advanced modern lock-in amplifiers (e.g. MFLi, Zurich Instruments), triggered by frequency sweeping event from the QCL, which is usually a TTL pulse.

Results

To demonstrate the feasibility of lock-in based PFIR microscopy, the first sample we measured was the polymer blend of polystyrene (PS) and polymethylmethacrylate (PMMA). The blend polymer sample was prepared by spin-coating the 30 mg/mL (PS:PMMA = 1:1.5) solution in toluene on a gold substrate. The spin-coater (KW-4A, Nanomicrotools) was set to 460 revolutions per minute (rpm) for 6 seconds and 1100 rpm for 60 seconds.

Figure 2 presents the measurement results with the topography of an area on the polymer blend in panel (a). Figure 2b displays the simultaneously collected adhesion through the PeakForce Tapping QNM. Figure 2c shows the lock-in collected PFIR signal at 1492 cm^{-1}, which is on resonance with the PS domain. Figure 2d shows the lock-in collected PFIR signal at 1724 cm^{-1}, which is on resonance with the PMMA domain. Figures 2c and 2d

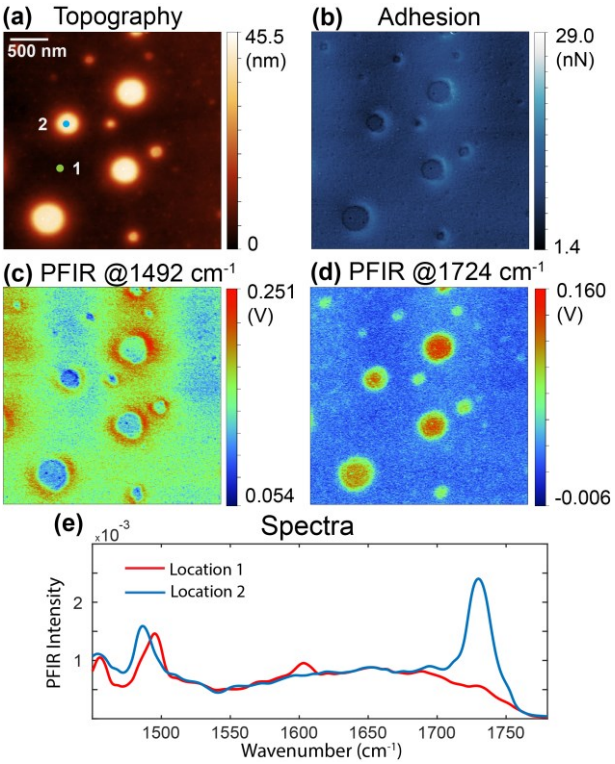

Figure 2. Lock-in PFIR imaging and spectroscopy of a PS:PMMA blend polymer film. (a,b) AFM topography and adhesion of the PS:PMMA blend polymer. (c,d) Lock-in PFIR images of the PS:PMMA blend polymer at 1492 cm^{-1} and 1724 cm^{-1} at the infrared absorption peaks of PS and PMMA, respectively. (e) PFIR spectra of the PS:PMMA blend polymer film. Wavenumbers 1450 cm^{-1} to 1678 cm^{-1} were measured with a higher laser power, and 1690 cm^{-1} to 1794 cm^{-1} were measured with a lower laser power to avoid signal saturation by PMMA. The blue and green marked spots on the topography image in panel (a) are the positions at which the spectra of PMMA (blue curve) and PS (red curve) domains were collected, correspondingly.

demonstrate that the lock-in based PFIR imaging can reveal the chemical distribution based on their IR signatures. Figure 2e

displays the collection of the lock-in based PFIR spectroscopy. The spectra were taken on the PMMA domain (dot region) and the PS domain (flat region). The spectra show a chemical contrast between the two domains. The wavenumber range of 1450 cm^{-1} to 1678 cm^{-1} was measured with a higher laser power to better visualize the peaks, and the range of 1690 cm^{-1} to 1794 cm^{-1} was measured at a lower power to avoid melting the PMMA at its stronger resonance signal.

Next, a block copolymer film sample was measured to demonstrate the technique. The block copolymer consisted of 7.5 mg/mL PS-*b*-PMMA (95-*b*-92, M_w/M_m = 1.10; P8537-SMMA, Polymer Source) in toluene solution. The block polymer was also spin-coated on a gold substrate using the same settings as the blend polymer. Figure 3a displays the topography of an area on the polymer blend. Figure 3b gives the simultaneously collected adhesion through the PeakForce Tapping QNM. Figure 3c shows the lock-in collected PFIR signal at 1493 cm^{-1}, which is in resonance with the PS domain. Figure 3d shows the lock-in collected PFIR signal at 1724 cm^{-1}, which is in resonance with the PMMA domain. Note that there was some scanner drift between the collection of 3c and 3d, which is possible for open-loop AFMs, like the Multimode 8 utilized here. Figures 3c and 3d agree with the PS:PMMA polymer blend results of Figure 2 in the sense that the lock-in based PFIR imaging can reveal the chemical distribution based on their IR signatures.

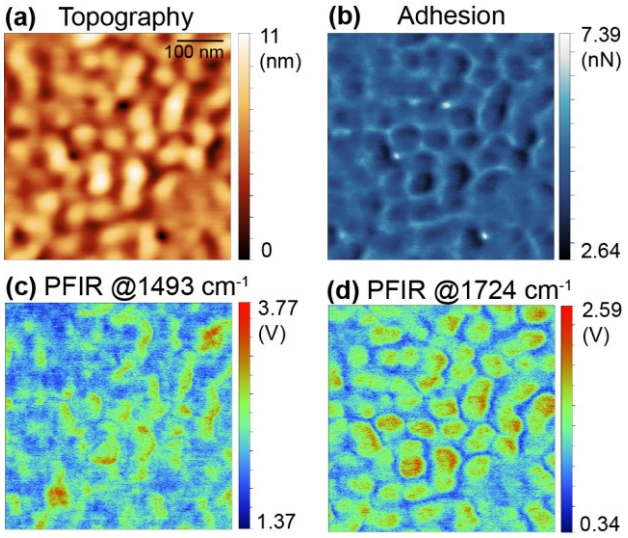

Figure 3. Lock-in PFIR imaging and spectroscopy of a PS-*b*-PMMA block copolymer film. (a,b) AFM topography and adhesion. (c,d) Lock-in based PFIR images at 1493 cm^{-1} and 1724 cm^{-1} at the infrared absorption peaks of PS and PMMA, respectively.

We also tested a representative biological sample of *E. coli*. The sample preparation was described in literature.[24] Figure 4 displays the measurement results. Figure 4a shows the topography of the *E. coli* cell. Figures 4b, 4c, and 4d display the lock-in collected PFIR images at 1552 cm^{-1}, 1644 cm^{-1}, and 1744 cm^{-1}. The wavenumber of 1552 cm^{-1} is in resonance with amide II of protein, 1644 cm^{-1} with amide I, and 1744 cm^{-1} with lipids. Figure 4e displays the lock-in collected spectrum at five different locations on the *E. coli* bacteria marked in Figure 4a. The measurement demonstrates the feasibility of lock-in based PFIR microscopy for other types of samples like biological ones.

Discussion

The advantage of lock-in based PFIR microscopy stems from its simplicity in instrument setup and ease of operation. The lock-in based PFIR implementation is much less complicated than for the regular PFIR one. The lock-in amplifier does both signal acquisition and signal processing of real-time collected mechanical signals without additional software/hardware programming, as required in regular PFIR microscopy. Compared to other lock-in based AFM-IR techniques, lock-in based PFIR microscopy inherits the advantages of PFT mode. The surface integrity of the sample is well preserved in PFT mode, in opposition to contact mode that leaves samples susceptible to deformation due to improper parameter settings. PFT mode is easy to operate with simple parameter settings, particularly with the Scanasyst® of peak force tapping mode. In contrast, PiFM or tapping mode AFM-IR requires setting up multiple operation parameters, such as a suitable tapping

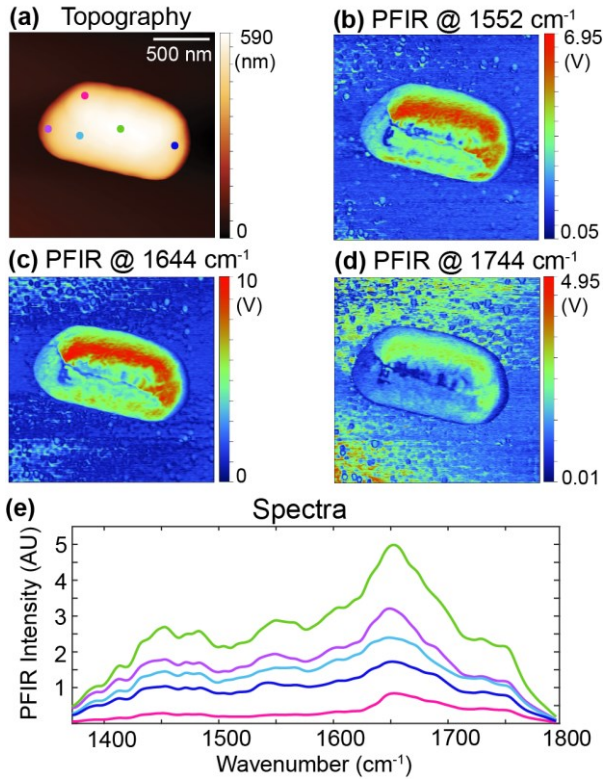

Figure 4. Lock-in PFIR imaging and spectroscopy of *E. coli*. (a) AFM topography of the *E. coli* bacteria. (b,c,d) Lock-in PFIR images of *E. coli* at 1552, 1644, and 1744 cm^{-1} under the infrared absorption peaks of amide II, amide I, and lipids, respectively. (e) PFIR spectra after spline smoothing of five locations on the *E. coli* bacteria in panel (a). The background is removed.

amplitude and adjustment of the repetition rate of the excitation lasers, which are critical to their successful operation.

While advantages present themselves in lock-in based PFIR microscopy, there are still deficiencies when compared to regular PFIR microscopy. The lock-in amplifier constantly acquires and processes the cantilever deflection signals during its operation, regardless of whether the tip is in contact or detached from the sample surface during the PFT cycle. The detached regime does not contribute to useful signal, although noise from the detachment regime still contributes to the noise background. However, only the contact regime contains useful sample-specific photothermal responses. Regular PFIR microscopy avoids this issue because the cantilever deflection signals from the detachment regime are not acquired, thus avoiding the contribution of noise to the signal. In lock-in based PFIR microscopy, such an increase in noise contribution is inevitable, imposing a trade-off between performance and instrumental complexity. In addition, the recently developed dual-color PFIR microscopy[24], allows two PFIR images to be collected simultaneously without relative drift. In the case of lock-in amplifier based PFIR microscopy, utilization of multiple IR sources is not straightforward, if possible, at all.

In our lock-in based PFIR microscopy, the laser emission is generated by a pack of TTL pulses described in Figure 2b. One can considered the TTL trigger pulses are created on a carrier frequency at the lock-in reference frequency, with the envelope determined by the PFT timing. The resulting photothermal expansion of the sample is phase-synchronized with the reference frequency from the lock-in amplifier. Therefore, the lock-in time constant can set at an arbitrarily long value to increase signal-to-noise ratio, albeit reducing the acquisition speed. The TTL reference frequency F is set at integer multiple of the PFT frequency *f,* so within each pack, there are integer number of trigger pulses with well-defined spacing at 1/F.

Conclusions

In summary, we have developed a lock-in based PFIR microscopy that simplifies the design of the original PFIR microscopy. We demonstrated this new method on nanostructured polymers and biological cells. The ease of setup and operation of a lock-in based PFIR microscopy will reduce the adoption barrier for PFIR microscopy as a nanoscale infrared chemical identification tool.

Author Contributions

X. G. X. generated the idea of lock-in based PFIR after discussion with M. W. Both X. G. X. and A.D. built the experimental setup. A.D. collected the data. Q. X. provided assistance during data collection. X.G.X and A. D. wrote the manuscript.

Conflicts of interest

M. W. is employed by Bruker Nano Surfaces Division, a manufacturer of instrumentation for AFM-based infrared spectroscopy. M.W and X.G.X. hold patents in AFM-based infrared spectroscopy.

Acknowledgments

We would like to thank Dr. Yan Yu for providing the E coli sample. X. G. X. would like to thank the support from the Beckman Young Investigator Award from the Arnold and Mabel Beckman Foundation and the Sloan Research Fellowship from the Alfred P. Sloan Foundation. A. D. Q. X. and X. G. X. would also like to thank the support from the National Science Foundation, award number CHE 1847765.

Notes and references

1. E. Abbe, *Archiv für Mikroskopische Anatomie*, 1873, **9**, 413-468.
2. A. Lahrech, R. Bachelot, P. Gleyzes and A. C. Boccara, *Opt. Lett.*, 1996, **21**, 1315-1317.
3. X. Chen, D. Hu, R. Mescall, G. You, D. N. Basov, Q. Dai and M. Liu, *Advanced Materials*, 2019, **31**, 1804774.
4. D. N. Basov, M. M. Fogler and F. J. García de Abajo, *Science*, 2016, **354**, aag1992.
5. M. S. Anderson, *Applied Spectroscopy*, 2000, **54**, 349-352.
6. A. Dazzi, R. Prazeres, F. Glotin and J. M. Ortega, *Optics Letters*, 2005, **30**, 2388-2390.
7. J. Mathurin, A. Deniset-Besseau, D. Bazin, E. Dartois, M. Wagner and A. Dazzi, *Journal of Applied Physics*, 2022, **131**, 010901.
8. A. Dazzi, C. B. Prater, Q. Hu, D. B. Chase, J. F. Rabolt and C. Marcott, *Applied Spectroscopy*, 2012, **66**, 1365-1384.
9. J. J. Schwartz, D. S. Jakob and A. Centrone, *Chemical Society Reviews*, 2022, **51**, 5248-5267.
10. D. Nowak, W. Morrison, H. K. Wickramasinghe, J. Jahng, E. Potma, L. Wan, R. Ruiz, T. R. Albrecht, K. Schmidt and J. Frommer, *Science Advances*, 2016, **2**, e1501571.
11. A. A. Sifat, J. Jahng and E. O. Potma, *Chemical Society Reviews*, 2022, **51**, 4208-4222.
12. J. Mathurin, E. Pancani, A. Deniset-Besseau, K. Kjoller, C. B. Prater, R. Gref and A. Dazzi, *Analyst*, 2018, **143**, 5940-5949.
13. L. Wang, H. Wang, M. Wagner, Y. Yan, D. S. Jakob and X. G. Xu, *Science Advances*, 2017, **3**, e1700255.
14. L. Wang, H. Wang and X. G. Xu, *Chemical Society Reviews*, 2022, **51**, 5268-5286.
15. D. S. Jakob, L. Wang, H. Wang and X. G. Xu, *Analytical Chemistry*, 2019, **91**, 8883-8890.
16. W. Li, H. Wang, X. G. Xu and Y. Yu, *Langmuir*, 2020, **36**, 6169-6177.
17. L. Wang, D. Huang, C. K. Chan, Y. J. Li and X. G. Xu, *Chemical Communications*, 2017, **53**, 7397-7400.
18. D. S. Jakob, H. Wang, G. Zeng, D. E. Otzen, Y. Yan and X. G. Xu, *Angewandte Chemie International Edition*, 2020, **59**, 16083-16090.
19. K. Ho, K. S. Kim, S. de Beer and G. C. Walker, *Langmuir*, 2021, **37**, 12723-12731.
20. H. Wang, J. M. González-Fialkowski, W. Li, Q. Xie, Y. Yu and X. G. Xu, *Analytical Chemistry*, 2021, **93**, 3567-3575.

21. H. Wang, E. Janzen, L. Wang, J. H. Edgar and X. G. Xu, *Nano Letters*, 2020, **20**, 3986-3991.
22. B. Pittenger, N. Erina and C. Su, *Application Note Veeco Instruments Inc*, 2010, **1**, 1-11.
23. A. Rosa-Zeiser, E. Weilandt, S. Hild and O. Marti, *Measurement Science and Technology*, 1997, **8**, 1333-1338.
24. Q. Xie, J. Wiemann, Y. Yu and X. G. Xu, *Analytical Chemistry*, 2022, **94**, 1425-1431.